LA-UR-16-29565
Approved for public release; distribution is unlimited.

Title: Uranium Hydride Nucleation and Growth Model FY'16 ESC Annual Report

Author(s): Hill, Mary Ann
Richards, Andrew Walter
Holby, Edward F.
Schulze, Roland K.

Intended for: Report

Issued: 2016-12-20

Uranium Hydride Nucleation and Growth Model

FY'16 ESC Annual Report

Mary Ann Hill, Andrew Richards, Ted Holby, and Roland Schulze
SIGMA Division

ABSTRACT
Uranium hydride corrosion is of great interest to the nuclear industry. Uranium reacts with water and/or hydrogen to form uranium hydride which adversely affects material performance. Hydride nucleation is influenced by thermal history, mechanical defects, oxide thickness, and chemical defects. Information has been gathered from past hydride experiments to formulate a uranium hydride model to be used in a Canned Subassembly (CSA) lifetime prediction model. This multi-scale computer modeling effort started in FY'13 and the fourth generation model is now complete. Additional high resolution experiments will be run to further test the model.

Introduction

The Uranium Hydride Model will be used in conjunction with other materials models as input to the gas transfer model, ChemPac, to predict the future aging of CSAs. Over the past several years, data from experiments has been used to formulate a uranium hydride model. Additional data has been collected from surveillance reports summarizing corrosion observations in LANL weapons systems and has recently been published in a report.[1] Data collected from this effort will be used for uranium hydride model validation.

The Version AR.4.0 Uranium Hydride Model

A new model of hydriding at uranium surfaces has been developed and integrated into ChemPaC. The new hydride model, so-called AR.4.0, is based on the experimental investigations conducted by R.K. Schulze and R.J. Hanrahan, who, in FY'15, proposed a 10-step mechanism to summarize their findings.[2]

Briefly, the model assumes that, to first order, the protective oxide layer of a uranium surface is impermeable, such that hydrogen ingress occurs only through defects in the oxide. It also assumes that pre-nucleated hydrides are plentiful in the near-surface bulk of the uranium, and that sites deeper than 50 microns are in a state of arrested growth due to volumetric constraints. During Rate I growth in the model, the so-called induction period, hydrogen ingress through an oxide layer defect is assumed to result in growth at a nearby (subsurface) hydride site; to first order, growth of the hydride is assumed spherical, until its diameter exceeds its initial depth, at which time the hydride ruptures the surface and Rate II Condon-Kirkpatrick growth kinetics[3-4] take over, with shape of the hydride governed by a phenomenological geometric factor [see Fig. 1b].

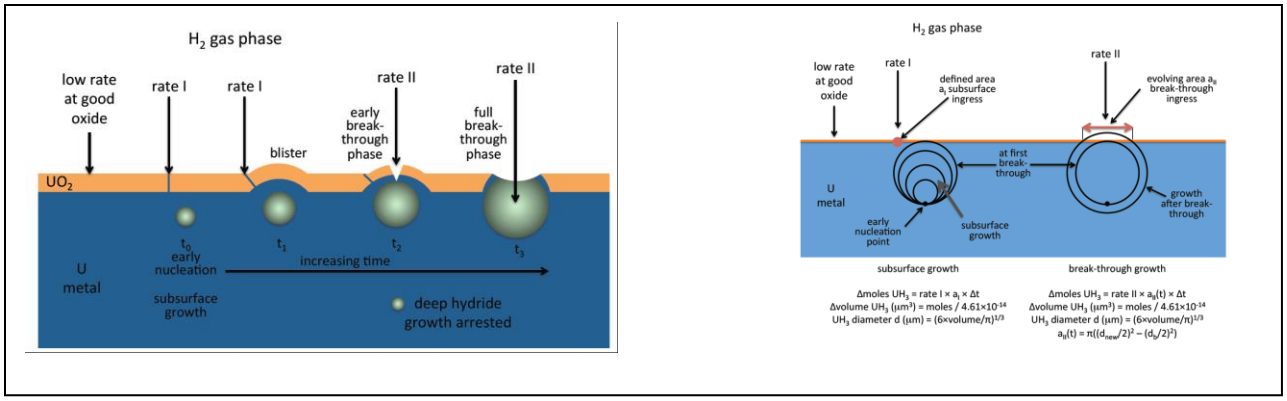

Figure 1: Depiction of 10-step growth model, and geometric growth factor.[2]

Transport of hydrogen to each hydride site, including dissociation at the oxide interface and diffusive transport through the bulk, is *not* explicitly modeled, but is instead captured by an effective hydride growth equation:

$$Rate\ I\ \left(\frac{moles\ UH_3\ formed}{cm^2\ sec}\right) = \begin{cases} 6.9 \times 10^{-8}\sqrt{P(torr)}, & P < 1\ torr \\ 1.3 \times 10^{-7}\sqrt{P(torr)} - 6.3 \times 10^{-8}, & P \geq 1\ torr \end{cases} \quad \text{(Eq. 1)}$$

$$Rate\ II\ \left(\frac{moles\ UH_3\ formed}{cm^2\ sec}\right) = \begin{cases} 6.3 \times 10^{-8}\sqrt{P(torr)}, & P < 1\ torr \\ 7.8 \times 10^{-8}\sqrt{P(torr)} - 1.6 \times 10^{-8}, & P \geq 1\ torr \end{cases} \quad \text{(Eq. 2)}$$

The tunable parameters of the 10-step model are the Phase I and Phase II hydride growth rate, which are modeled as having a square-root dependence on the partial pressure of hydrogen at the uranium surface, the defect density per unit area in the oxide layer, and the initial depth and diameter of the (subsurface) prenucleated site associated with an oxide defect. Each of these parameters, in theory, is a measurable material property. Initial estimates of the kinetic parameters were estimated in the aforementioned investigations by Schulze & Hanrahan[2]:
Oxide defect area = 1.0 e-15 m^2
Depth of pre-nucleated hydride = 30.0 e-6 m
Defect density = 1.0 e-4 defects/m^2
A Poisson sampler was used to generate the locations of the oxide defects. All hydrides in the preliminary simulations have the same initial defect area and starting depth. The theoretical bounds on these parameters are being developed from first-principles DFT simulations, conducted by T. Holby.

The numerical implementation of the 10-step model in ChemPaC uses a pseudo-random seed to generate a list of spatial locations of oxide defects along a uranium surface, as well as the initial depths and diameters of the associated pre-nucleated sites, thereby circumventing the need for an explicit model of hydride nucleation. Since this seeding is done as a pre-processing step, the implementation appears to be quite efficient. Preliminary results from ChemPaC, using order-of-magnitude estimates for the model parameters were acquired.

AR.4.0 was qualitatively compared with model JT.2.0 developed by J. Tanksi in FY'14.[5] It was found that seemingly disparate parameters in the two models serve similar functions, and result in similar

behavior. The key difference appears to be the explicit, physics-based modeling of the subsurface growth regime, i.e. the induction period, incorporated into the 10-step model, in contrast to the phenomenological "appearance" function used in the JT.2.0 model, which was essentially a modified ramp function. JT.3.0 incorporated subsurface hydriding.[5] Both the JT.2.0 and 10-step models use a phenomenological geometric factor to describe the evolution of the shape of the model. The new 10-step model, however, uses far fewer tunable parameters, and parameters which are present have reasonably intuitive physical interpretations, which are relatively decoupled.

Density Functional Theory Modeling

Great progress was made in FY16 elucidating the thermodynamic and kinetic behavior of H atoms in the α-U lattice using quantum chemical modeling (in particular, density functional theory, DFT, for internal energy calculations and the nudged elastic band, NEB, methodology for diffusion barrier calculations). This year's efforts focused on the kinetics of H interstitial diffusion and response to uniaxial elastic strain, thermodynamics of H-clustering / H-H interactions, U-vacancy diffusion, U-vacancy and H thermodynamics, and kinetics of U-vacancy and H co-diffusion. The calculated values were found to have implications for possible mechanisms governing the phase transformation of α-U to UH_3.

Previous efforts from FY15 considered hydrostatic elastic strain effects on H diffusion between interstitial square-pyramidal (sqpy) low-energy binding sites in the (100) crystallographic direction, identifying compressive strain as decreasing calculated diffusion coefficient values and tensile strain as increasing calculated diffusion coefficient values.[6] In FY16, calculations of the impact on diffusion barrier for uniaxial elastic strain were completed. Directions of applied strain perpendicular to the diffusion pathway included the (010) and (001) directions and the same trends as those found for the hydrostatic case were determined. For uniaxial elastic strain applied along the (100) diffusion direction, the opposite trend was found with compressive strain decreasing calculated diffusion barrier and tensile strain increasing the calculated barrier. This finding exemplified further the complex interrelation of elastic strain and interstitial diffusion kinetics in an orthorhombic crystal structure.

The attractive behavior between neighboring interstitial H atoms was another example of previously unreported behavior in the U-H system discovered via quantum chemical modeling in FY16. Previous DFT studies[7] suggested that interstitial H did not interact and so values of lone-H binding energies were utilized for determining H solubility in the undefected α-U lattice. Calculation of binding energies for a sampling of clustered-H configurations showed that certain organizations of H (including sqpy and tetragonal positions along the (100) crystallographic direction) stabilized the binding energy per H interstitial by up to 0.13 eV/H (0.19 eV/H for a $U_{64}H_{16}$ cell, Figure 2a *vs.* 0.32 eV/H for the lone-H $U_{64}H$ cell, Figure 2b) in fixed volume periodic structures. This finding was attributed to a cooperative strain effect.

a b

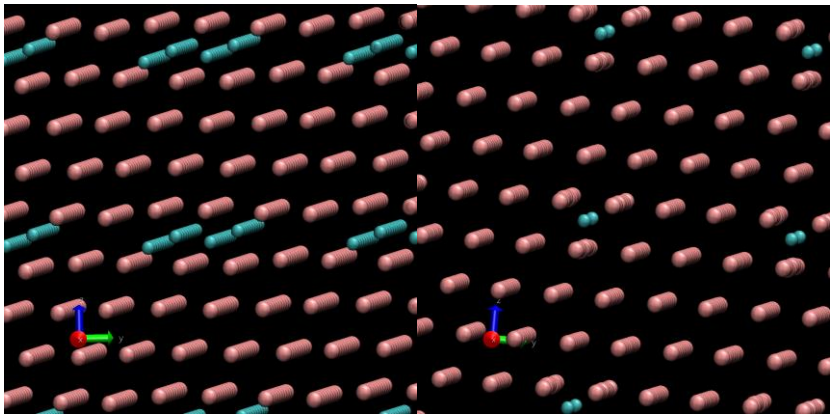

Figure 2. Supercell depiction of relaxed (a) $U_{64}H_{16}$ cell and (b) $U_{64}H$ structures. Bronze spheres represent U and cyan spheres represent H.

Due to the large increase in volume associated with the α-U to UH_3 phase transformation, it was posited that the kinetics of the phase transition may depend on U-vacancy diffusion to the nucleation/growth site in addition to H-diffusion to the site. To consider this possibility, directionally dependent U-vacancy diffusion barriers were calculated. A directional dependence similar to H-interstitial diffusion was found with again the (100) direction being both percolating and having the lowest calculated barrier (0.20 eV). This calculated barrier was found to be significantly below the calculated barrier for interstitial H-diffusion (0.35 eV) suggesting that U-vacancies are more mobile under low-temperature conditions than interstitial H. As such, a mechanism in which U-vacancies diffuse to interstitial H can be considered. Such U-vacancy/H defects were calculated to have a formation-energy of 1.36 eV compared to the U-vacancy formation energy of 1.77 eV. These values suggest that if a U-vacancy exists, that it is stabilized by the binding of H at the vacancy site and such vacancies thermodynamically act as traps for interstitial H atoms. Considering H diffusion into and out of these trap-sites from and to neighboring sqpy sites gave barrier values of 0.20 eV and 0.94 eV, respectively. These values suggest it is a relatively low barrier process for H to enter the vacancy site and a relatively high barrier process to leave the vacancy site, confirming that the site acts as a trap for H kinetically. Finally, the co-diffusion of a U-vacancy with bound H was considered. A barrier of 0.89 eV was calculated, a value similar to the barrier associated with H diffusing out of the U-vacancy site. This again suggests that once the vacancy-H defect structure has been generated, there are significant barriers for it to dissociate or diffuse. The vacancy-diffusion mediated mechanism for UH_3 formation in bulk along with attractive H-H interactions may explain the anomalously large barriers in the formation pathway previously posited for the phase transition.[7]

In addition to these findings, Model TH.1 was successfully incorporated into the Uranium Hydride model. This model included temperature-dependent diffusion coefficients for interstitial H in the undefected α-U lattice calculated using computational quantum chemistry (density functional theory and nudged-elastic-band methods) and comparisons to available experimentally derived values.

The High Sensitivity Reactor for Uranium Hydriding Experiments

In addition to surveillance data, data collected from experiments using a high sensitivity reactor will be used for testing of the model. This past year a prototype reactor was built, shown in Fig. 3. This reactor is constructed for use in an ultrahigh vacuum (UHV) environment and has two sensitivity pressure scales, 1 torr and 1000 torr. The 1 torr baratron differential pressure transducer is for monitoring the subsurface hydride growth phase while the 1000 torr baratron absolute pressure transducer monitors reaction rate following hydride breakthrough. Hydrogen pressures up to 1000 torr will be used for accelerated reaction rates. An optical viewport on the cell can be used for optical microscopy. Time of breakthrough will be correlated to gas reaction rates.

Figure 3. High sensitivity reactor.

Future Work

In the upcoming year, corrosion signatures will be determined based upon surveillance results to achieve a better understanding of the vulnerability of specific locations to corrosion in a CSA. A comparison of uranium hydride models AR4.0 and JT3.0, incorporating subsurface hydriding, will be completed. Parameter studies and sensitivity analyses of model parameters are planned. Feasibility studies for investigating the direct experimental measurement of oxide defect densities and nucleation site depths will be researched. A more detailed phase diagram will be generated for structures between the α-U and UH_3 structures with and without volumetric relaxation, following the example of Ong et al.[8] Such a phase diagram would provide valuable insight into stable or meta-stable structures relevant for transition pathways between the two phases which current DFT-based models have not captured. Experiments will be conducted using the high sensitivity reactor to acquire test data for the Uranium Hydride model.

REFERENCES

1. M.A.Hill, (U) A Survey of CSA Corrosion Observation in LANL Weapons Systems, Los Alamos National Laboratory report LA-14490 (2016) 267 pages.
2. R. K. Schulze and R. J. Hanrahan, unpublished research, 2015.
3. J. R. Kirkpatrick and J.B. Condon, The linear solution for hydriding of uranium, J. Less Common Metals, **172-174** (1991) 124-125.
4. G. L. Powell, W. L. Harper, and J. R. Kirkpatrick, The kinetics of the hydriding of uranium metal, J. Less Common Metals, **172-174** (1991) 116-123.

5. J. A. Tanski, M. A. Hill, and E. F. Holby, (U) Development of a Uranium Hydride Model," Los Alamos National Laboratory report LA-CP-15-01161 (2015).
6. E. F. Holby, Crystallographic Orientation Effect on Hydrogen Diffusion in α-Uranium via DFT, LA-UR-16-20613, in final preparation (2016).
7. C. D. Taylor, T. Lookman, and R. S. Lillard, Ab initio calculations of the uranium-hydrogen system: Thermodynamics, hydrogen saturation of α-U and phase transformation to UH3, Acta Mater **58** (2010) 1045-1055.
8. S. Ping Ong, L. Wang, B. Kang, and G. Ceder, Li-Fe-P-O2 Phase Diagram from First Principles Calculations, Chemistry of Materials **20** (2008) 1798-1807.